Synthetic Metals 260 (2020) 116261

Contents lists available at ScienceDirect

Synthetic Metals

journal homepage: www.elsevier.com/locate/synmet

Photoemission studies of C8-BTBT/$La_{0.67}Sr_{0.33}MnO_3$ interface

Haipeng Xie[a], Dongmei Niu[a,*], Yuan Zhao[a], Shitang Wang[a], Baoxing Liu[a], Yuquan Liu[a], Han Huang[a], Peng Wang[b], Di Wu[b], Yongli Gao[a,c,*]

[a] Hunan Key Laboratory of Super Microstructure and Ultrafast Process, School of Physics and Electronics, Central South University, Changsha, Hunan, 410083, PR China
[b] National Laboratory of Solid State Microstructures and Department of Physics, Nanjing University, Nanjing, 210093, PR China
[c] Department of Physics and Astronomy, University of Rochester, Rochester, NY, 14627, USA

ARTICLE INFO

Keywords:
Photoemission spectroscopy
Electronic structure
LSMO
C8-BTBT

ABSTRACT

The electronic structure and chemical reaction at the interface between 2,7-diocty[1]benzothieno[3,2-b]benzothiophene (C8-BTBT) and $La_{0.67}Sr_{0.33}MnO_3$ (LSMO) have been investigated using ultraviolet photoemission spectroscopy, X-ray photoemission spectroscopy, and atomic force microscopy. There is an interface dipole of 0.41 eV, pointing from LSMO to C8-BTBT. The Fermi level is 1.64 eV above the highest occupied molecular orbital (HOMO) of C8-BTBT and the injection of electron from LSMO to C8-BTBT is not efficient. The oxygen is found to diffuse from LSMO to C8-BTBT, which leads to the Mn^{4+} reduced into Mn^{3+} at the C8-BTBT/LSMO interface. The growth mode of C8-BTBT on LSMO film is Stranski-Krastanov(SK)mode. Our investigation suggest a buffer layer between the C8-BTBT and LSMO to bridge the electron transport barrier.

1. Introduction

Organic semiconductors (OSCs), including π–conjugated polymers and small molecules, have been a vibrant field of research and development due to the rich physics, flexible chemistry, and cost efficiency [1–3]. In spin related devices, π–conjugated polymers have been used as an organic layer between two ferromagnetic (FM) electrodes in organic spin valves [4,5]. The spin polarization carriers injected from the electrode into the OSCs has been proved using low-energy muon spin rotation and two-photon photoemission spectroscopy [6–9]. Transport of spin polarized carriers from the first FM electrode to the second depends on the properties of the organic semiconductors. The carrier mobility is one of the important factors for the device performance. The spin diffusion length, λ_s, is related to the carrier mobility μ according to the relationship of $\lambda_s = \sqrt{\mu k_B T \tau / e}$, where k_B, T, τ, and e are the Boltzmann constant, temperature, spin relaxation time, and electron charge, respectively [10–13]. The relatively low mobility of OSC materials often limits the spin diffusion length in OSCs, which has been an obvious obstacle for observing the spin precession or Hanle effect in those materials [14,15].

The relatively low carrier mobility of π–conjugated materials was generally caused by charge hopping/tunneling transport mechanism. Recently, Yuan et al. demonstrated in 2,7-diocty[1]benzothieno[3,2-b]benzothiophene (C8-BTBT) thin films a field effect mobility up to 43 $cm^2 V^{-1} s^{-1}$ by using a novel off-center spin-coating technique [16]. High-performance C8-BTBT-based devices have since been obtained by different film preparation methods and device geometries [17–20]. The band-like transportation may be the reason of the high carrier mobility in the C8-BTBT film [21], which can also make C8-BTBT a good candidate for organic spintronic devices. The half-metallic manganite $La_{0.67}Sr_{0.33}MnO_3$ (LSMO) is often used as ferromagnetic electrode due to its 100 % spin polarization at the Fermi level and stability against oxidation [22–26]. In addition, the Curie temperature of LSMO films lies above room temperature if prepared with suitable deposition parameters [27,28]. It is well known that the charge transport across organic/metal interface is important for optimum device operation and the understanding of these interfaces has tremendous impact on the semiconductor device technology. It is meaningful to understand the interfacial interaction and electronic structure of the interface between C8-BTBT and LSMO, and decide if it is suitable for related devices.

In this work, we report our investigation on the interface formation of C8-BTBT/LSMO using ultraviolet photoemission spectroscopy (UPS), X-ray photoemission spectroscopy (XPS), and atomic force microscopy (AFM). We found that the C8-BTBT film exhibited Stranski-Krastanov (SK)mode on LSMO. The Fermi level at the interface is close to the mid-gap position of C8-BTBT, which sets a limit to charge injection from LSMO. The oxygen diffuses from LSMO to C8-BTBT and makes Mn^{4+} reduced to Mn^{3+} in the C8-BTBT/LSMO interface, and then reacts with

* Corresponding authors at: Hunan Key Laboratory of Super Microstructure and Ultrafast Process, School of Physics and Electronics, Central South University, Changsha, Hunan 410083, PR China.
E-mail addresses: mayee@csu.edu.cn (D. Niu), ygao@csu.edu.cn (Y. Gao).

https://doi.org/10.1016/j.synthmet.2019.116261
Received 21 June 2019; Received in revised form 26 November 2019; Accepted 2 December 2019
Available online 25 December 2019
0379-6779/

the C8-BTBT under the ultraviolet light. Our results suggest that direct injection of spin from LSMO to C8-BTBT by charge carriers may not be efficient, and interface modification are required to design C8-BTBT/LSMO-based devices.

2. Experimental details

The UPS and XPS measurements were performed in an ultrahigh vacuum (UHV) system equipped with a spectrometer chamber, an in situ organic evaporation chamber, and a sputtering chamber. The base pressure of the spectrometer chamber, organic evaporation chamber, and sputtering chamber is $\sim 1.5 \times 10^{-10}$ mbar, 1×10^{-9} mbar and 3×10^{-8} mbar, respectively. The spectrometer chamber includes a SPECS PHOIBOS 150 hemispherical energy analyzer. The UPS was measured with a SPECS Microwave UV Light Source (He I = 21.2 eV), and the XPS with a monochromatic SPECS XR-MF X-ray source (Al K_α = 1486.7 eV). The UPS spectra were collected with the samples biased at −5.0 eV to observe the low energy secondary cut-off. The UV light spot is about 1 mm in diameter. A total energy resolution of 70 meV was determined from the Fermi edge of Au. The binding energies of all UPS and XPS spectra were calibrated and referenced to the E_F of the sample. The LSMO substrate was grown by pulsed laser deposition on $SrTiO_3$ (001) substrates [29]. After being cleaned in ultrasonic baths of acetone and ethanol for 15 min, respectively, the LSMO substrate was inserted into the sputtering chamber and annealed at 5×10^{-5} mbar oxygen atmosphere for 120 min at 450 °C, and the quality was verified by UPS, XPS, and low energy electron diffraction (LEED) image. The results show that the LSMO substrate is clean and well crystallized after annealing in oxygen [30]. After natural cooling, the LSMO substrate was transferred to the organic evaporation chamber and the pressure is $\sim 3 \times 10^{-8}$ mbar in the transfer process. The C8-BTBT molecule was thermally evaporated at the deposition rate of 1 − 2 Å/min and its thickness was monitored with a quartz crystal microbalance (QCM). Atomic force microscopy (AFM) imaging was examined by Agilent 5500AFM/SPM using the tapping mode. All measurements were taken at room temperature.

3. Results and discussion

The UPS spectra of C8-BTBT on LSMO are presented as a function of the thickness of C8-BTBT over layer in Fig. 1. All the spectra are normalized to the same height for visual clarity. Fig. 1(a) shows the cut-off region of the UPS data. The work function (WF) was determined by the center of the slopes of the spectra. The WF of LSMO is 4.70 eV, which is in agreement with previous reports [31–33]. The WF of 5 Å C8-BTBT film is 4.29 eV and that of 120 Å C8-BTBT film is 3.72 eV. A total WF decrease of about 0.57 eV is observed. The HOMO region of the UPS spectra is shown in Fig. 1(b) and (c). We notice that the HOMO of C8-BTBT shift towards the higher binding energy (BE) with increasing C8-BTBT thickness and the total shift is about 0.24 eV. As the thickness increase from 5 to 120 Å, The HOMO onset of C8-BTBT film increases from 1.64 to 1.88 eV, indicates that the HOMO moves away from the Fermi level (E_F) slightly. As shown in Fig. 1(b), there are three characteristic peaks (P1, P2, P3) from C8-BTBT. Peak P1, P2, and P3 of 10 Å C8-BTBT are located at ca. 6.61 eV, 9.28 eV, and 10.63 eV respectively. All of these peaks shift toward high binding energy rigidly as the C8-BTBT thickness increases from 10 to 40 Å. The rigid shift is also reflected in that of the cut-off. At 80 and 120 Å C8-BTBT, we observed that the cut-off edge became wider markedly and the characteristic peak of HOMO between 1.5–3.0 eV disappeared, while P1, and P2 showed a larger shift. The shift and broadening lead us to deduce that there are charging effects when 80 and 120 Å C8-BTBT are deposited on the LSMO substrate. On the other hand, we found that the changes in the offset of WF and P1 or P2 were different for the two coverages. The shift for 120 Å C8-BTBT is 1.41 eV for P1 and P2, in comparison to that of 10 Å C8-BTBT, while that of the cut-off is merely 0.43 eV. The non-rigid shifts and the disappearance of the HOMO features indicate that there are more than just charging. We attribute these changes to the altering orientation of the C8-BTBT molecular from flat lying to standing, as previously observed in other C8-BTBT interfaces [34–37].

To highlight the effect of the C8-BTBT thickness on the energy level shift, we plot the energy levels alignment diagram for the C8-BTBT/LSMO interface as shown in Fig. 1(d). Taking the 3.84 eV energy gap of C8-BTBT into consideration [38], the Fermi level lies near mid-gap position of C8-BTBT at the interface. The electron injection barrier from LSMO to C8-BTBT is about 2.20 eV and the hole injection barrier is 1.64 eV, which means that the spin related injection is not efficient. There is an interfacial dipole of 0.41 eV pointing from LSMO to C8-BTBT side. The WF decreases by 0.26 eV from 4.29 eV at 5 Å to 4.03 eV at 40 Å, while the HOMO decreases by 0.15 eV from 5 to 40 Å. We can see a clear band bending where the WF and HOMO shows similar downward shift as the increasing of the C8-BTBT thickness, which can be attributed to the charge redistribution and interfacial interaction at C8-BTBT/LSMO interface.

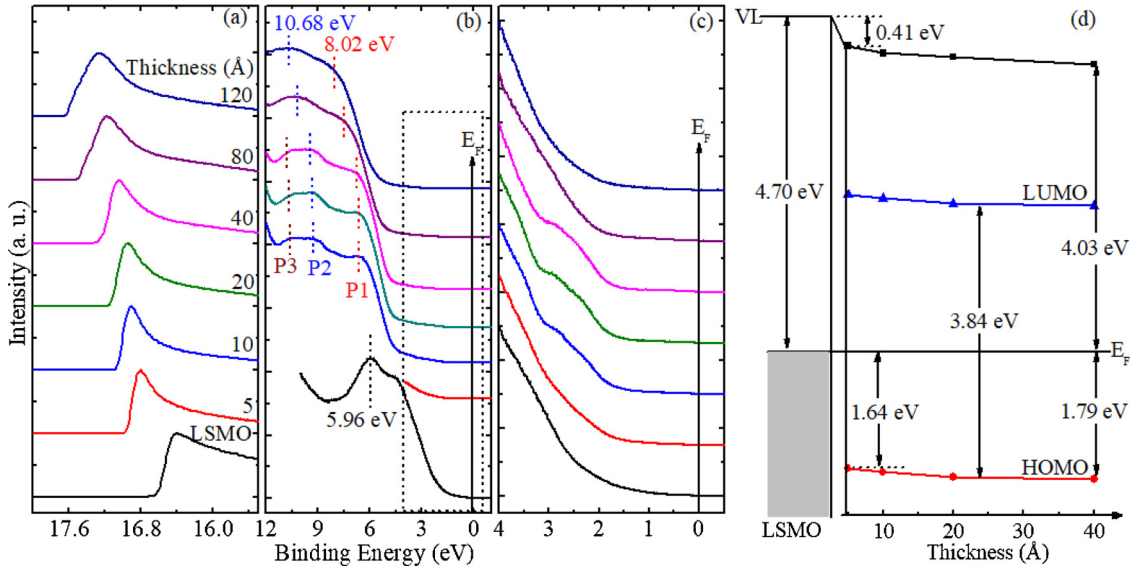

Fig. 1. UPS spectra evolution of C8-BTBT thickness deposited on LSMO. (a) Cut-off region, (b) HOMO region, (c) Magnified at binding energy between -0.5 eV to 4 eV, (d) Evolutions of the WF, HOMO, and LUMO as the C8-BTBT thickness increases.

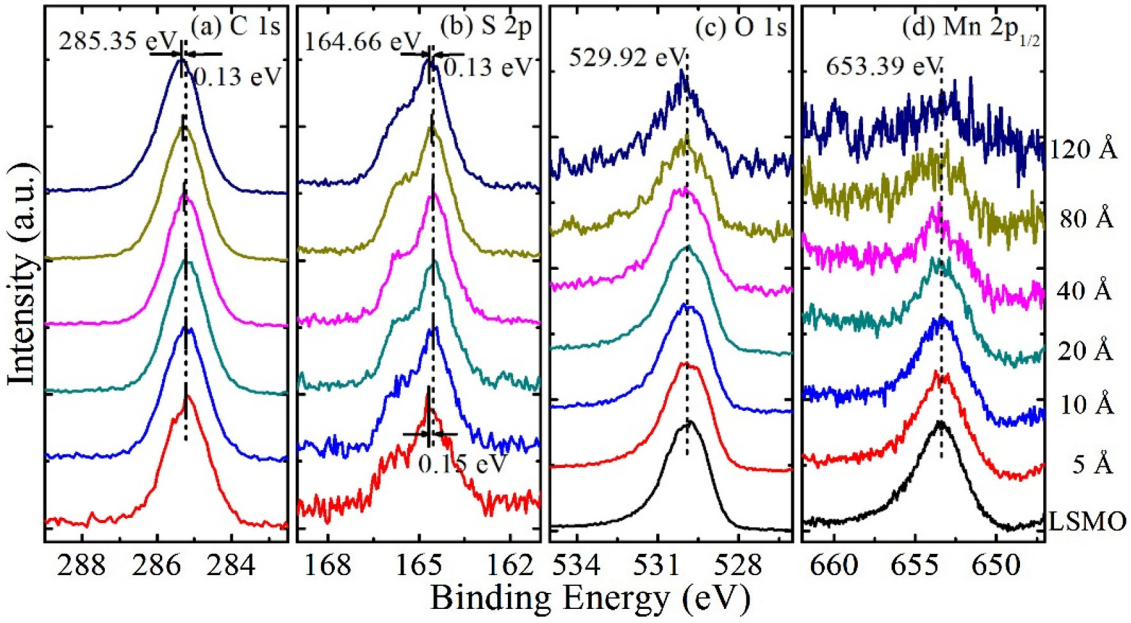

Fig. 2. XPS spectra of (a) C 1s, (b)S 2p, (c) O 1s, and (d) Mn $2p_{1/2}$ at different over layer C8-BTBT thickness. Note: XPS test after UPS test.

Presented in Fig. 2 is the evolution of C 1s, S 2p, O 1s, and Mn $2p_{1/2}$ peaks as a function of increasing C8-BTBT thickness. All the spectra are normalized to the same height for visual clarity. At the initial C8-BTBT deposition, the C 1s peak is located at 285.22 eV as shown in Fig. 2(a). With increasing of the C8-BTBT film, the C 1s peak moves to 285.35 eV at 120 Å and the total shift is ca. 0.13 eV. The C 1s core level is fitted with commercial software CasaXPS (see supporting information Fig. S1), which shows that the shift of C ls and S 2p core level is little. As shown in Fig. 2(b), the S $2p_{3/2}$ peak shifts from 164.68 eV at 5 Å to 164.53 eV at 10 Å, which is different from those in the C 1s and UPS data. Meanwhile, the S $2p_{3/2}$ peak moves to 164.66 eV at 120 Å and the total shift is ca. 0.13 eV. The O 1s and Mn $2p_{1/2}$ from the LSMO substrate are shown in Fig. 2(c) and (d). We can see the position of peak do not shift as the C8-BTBT thickness increases, indicates that the LSMO is not affected appreciably by the C8-BTBT film. The O 1s and Mn $2p_{1/2}$ spectra can still be observed when the C8-BTBT film thickness reach 120 Å, indicating that the growth mode of C8-BTBT molecules are either Volmer-Weber(VM) or Stranski-Krastanov(SK)mode on the LSMO substrate.

Generally, the growth mode can be related to the intensity attenuation of photoelectrons from the C8-BTBT overlayer or the LSMO substrate. Details about this could be found elsewhere [39,40]. As shown in Fig. 3, the intensities of the photoelectrons ejected from the O 1s and Mn 2p decrease as the increasing of C8- BTBT thickness and it can be divided into three different regions. In the first region, the intensities of the photoelectrons decrease quickly from 0 to 10 Å, indicated that the growth mode in this region is Frank-van der Merwe model. In the last region, the intensities of the photoelectrons slow decreases from 40 to 120 Å, which is a typical island mode. There is a transition region for the intermediate region. Shown in Fig. 4(d) is the AFM image of 120 Å C8-BTBT film deposited on LSMO. We found that 120 Å C8-BTBT film did not cover the LSMO substrate, indicated that the C8-BTBT molecules exhibited Stranski-Krastanov (SK) mode as grown on the LSMO substrate.

It is instructive to compare the C 1s of 40 Å C8-BTBT film deposited on different substrates, as shown in Fig. 4(a). The C 1s peaks of 40 Å C8-BTBT film deposited on SiO_2, Cu, Ni show the same binding energies (~284.97 eV) [34,40,41], which can be attribute to the intrinsic binding energy for C8-BTBT molecule. When 40 Å C8-BTBT film deposited on LSMO substrate, the C 1s peak located at ca. 285.26 eV which is higher than those on SiO_2, Cu, Ni substrate. The possible

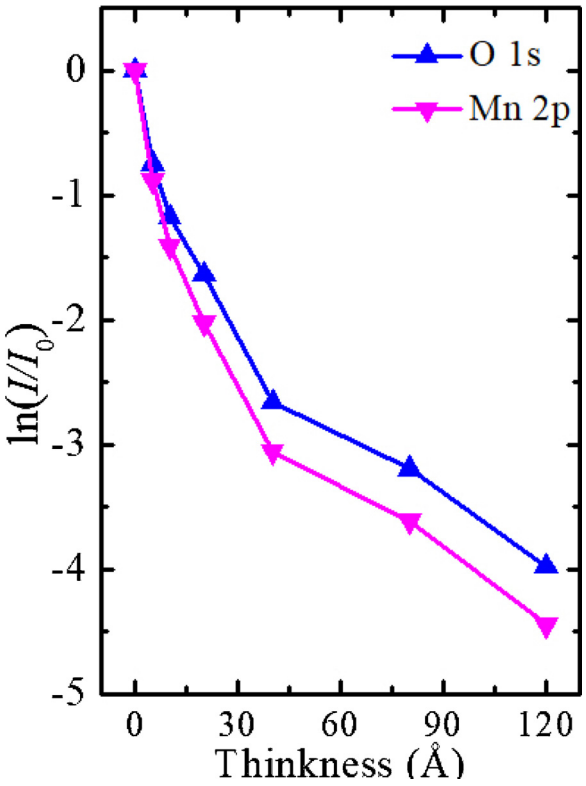

Fig. 3. The function relationship between the photoelectron intensity and the thickness of C8-BTBT film. I_0 is the photoelectron intensities from the LSMO substrate without the C8-BTBT overlayer.

reasons is that some interfacial interaction taking place at C8-BTBT/LSMO interface. We then carefully checked the Mn $2p_{1/2}$ spectra for compare. As shown in Fig. 4(b), the dot lines are fitted with commercial software CasaXPS. The magnetic properties of LSMO are mainly determined by Mn valence state, which can be described as a mixture of Mn^{3+} and Mn^{4+} making up a Mn^{3+}-O-Mn^{4+} bond [42–45]. The Mn $2p_{1/2}$-related peaks at 653.17 eV and 654.67 eV are assigned to Mn^{3+} and Mn^{4+}, respectively [42,43,46]. We found that the Mn^{4+} decreases

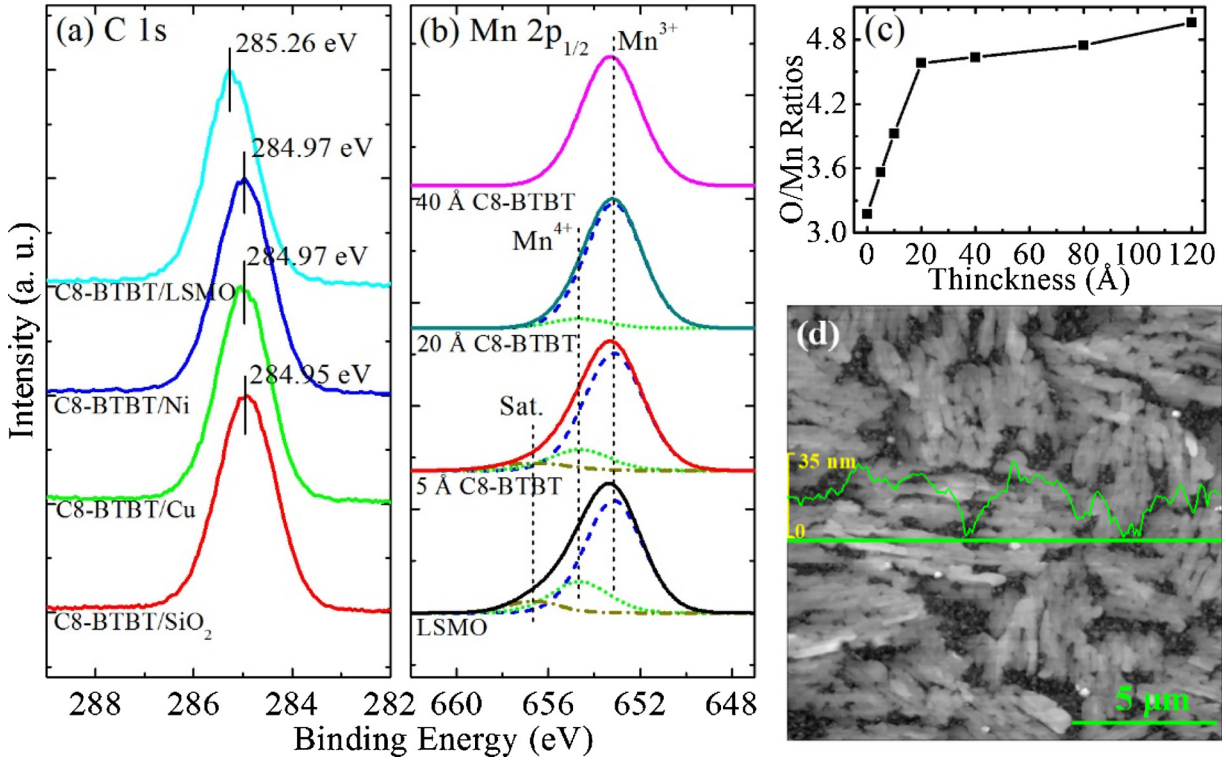

Fig. 4. (a) The C 1s of 40 Å C8-BTBT film deposited on different substrates. (b) The Mn $2p_{1/2}$ spectra evolution of C8-BTBT thickness deposited on LSMO. (c) The atomic ratio of O/Mn. (d) AFM image of 120 Å C8-BTBT film deposited on LSMO.

with the C8-BTBT film thickness increasing and disappears at 40 Å C8-BTBT film, indicating the strong reduction of Mn^{4+}.

In addition, we examined the ratio of O/Mn of LSMO covered by C8-BTBT film, as shown in Fig. 4(c), and found the O/Mn ratio increasesed with the C8-BTBT film thickness. The possible reason should be the diffusion of oxygen to the upper C8-BTBT film which makes the detection efficiency of oxygen higher than that of the Mn ions. Shown in Fig. 4, the Mn^{4+} decreases while the ratio of O/Mn increases with the increasing C8-BTBT film thickness. As both Mn and O are from the substrate, it is natural to deduce that the reduction of Mn and increase of O indicate oxygen out-diffusion into C8BTBT. Another evidence supporting the oxygen out-diffusion model is that the O/Mn ratio increase quicker than the reduction of Mn^{3+} at low C8-BTBT coverages, which is understandable from the finite detection depth of XPS. Combining the disappearing of Mn^{4+} and the increasing O/Mn ratio, it is reasonable to infer that the diffusion of O from LSMO to the interface makes Mn^{4+} reduced to Mn^{3+} in the C8-BTBT/LSMO interface. The HOMO bending of C8-BTBT/LSMO can also be attributed to the O diffusion to C8-BTBT which lift the Fermi level of C8-BTBT. We have observed similar oxygen accumulation at the interface of C_{60}/LSMO [30]. The type of the OSC seems have little impact of the diffusion of oxygen from inside of LSMO to the surface as the C8-BTBT is a typical *p*-type OSC and C_{60} typical *n*-type. We also find there is a plateau of O/Mn ratio at 20 Å. As shown in Fig. 3, the growth mode is Frank-van der Merwe model from 0 to10 Å and island mode from 40 to 120 Å. The film did not cover the LSMO substrate, as shown in Fig. 4(d). So we assume that the C8-BTBT islands appear and growth from 10 Å to 40 Å and the 20 Å is a critical point. There is layer-plus-island before 20 Å and only island after 20 Å. Thus, the transition of O/Mn ratio at 20 Å can be attributed to the change of the growth mode of C8-BTBT.

As shown in supporting information Table S1, the C/S ratio also has been examined. We found that the C/S ratio is ca. 13.55 and almost keep unchanged as the increase of C8-BTBT thickness after UPS test. The C/S ratio is ca. 14.25 and ca. 14.51 for 80 and 120 Å C8-BTBT respectively before UPS test, which is close to the stoichiometry ratio of C8-BTBT. It is indicated that the structure of the C8-BTBT molecule deposition on LSMO substrate is stable before UPS test and the C8-BTBT molecule is lying down with the long c-axis parallel to the surface [47].

We also noticed the UV light induced core levels shifts of the XPS by examining the XPS before and after UPS test. Shown in Fig. 5 are the XPS spectra of 80 Å and 120 Å C8-BTBT thickness before and after UPS test. The UPS and XPS measurements were taken in situ one after another. As shown in Fig. 5(a) and (b), the C 1s core level include one peak which located at ca. 285.17 eV and ca. 285.29 eV for 80 and 120 Å C8-BTBT respectively before UPS test. After UPS test, the shape and position of both C 1s and S 2p changed slightly. A weak component of C 1s which located at ca. 286.12 eV for 80 Å and 286.18 eV for 120 Å appears at the left side (higher binding energy) of the main peaks and shows a slightly shift toward higher binding energy after UPS test. The S 2p core level is a doublet consisting of S $2p_{3/2}$ and S $2p_{1/2}$ components with an energy separation of 1.2 eV and a branching ratio of 2 [48,49]. As shown in Fig. 5(a) and (b), the S $2p_{3/2}$ core level are located at ca. 164.02 eV and ca. 164.22 eV for 80 Å and 120 Å C8-BTBT respectively before UPS test. Contrary to C, a new component appears at right side (low binding energy) after UPS test. The new component are located at ca. 163.63 eV and ca. 163.73 eV for 80 Å and 120 Å C8-BTBT respectively. For the new component appear after UPS test, the possible reason is that UPS test affect the C8-BTBT molecules.

We have not observed the changes of C 1s and S 2p from the C8-BTBT on other substrate such as SiO_2, Ni, Cu [34,40,41]. So it is not likely that the UV light caused the photo chemical reaction of C8-BTBT itself. It is reasonable to attribute the present changes to the participation of oxygen diffuse from LSMO in this photo chemical process. In addition, the interfacial interaction between C8-BTBT molecule and LSMO substrate before and after UPS test should also be considered. We checked the O 1s and Mn $2p_{1/2}$ from the LSMO substrate carefully, as shown in Fig. 5(c) and (d). We found that the peak position of O 1s and Mn $2p_{1/2}$ do not shift after UPS test, which indicates that it is not likely that chemical reaction take place directly between LSMO substrate and C8-BTBT molecule. It is probably oxygen released from the LSMO

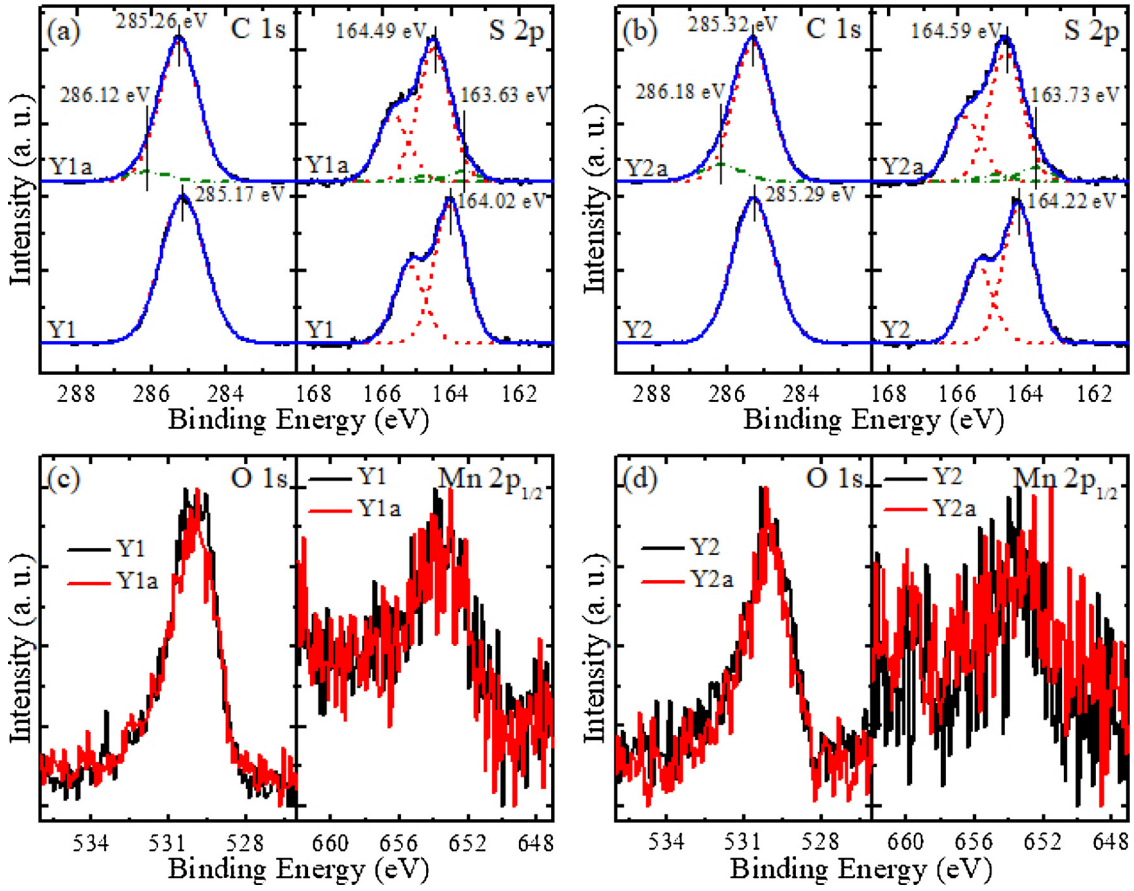

Fig. 5. The C 1s and S 2p of (a) 80 Å and (b) 120 Å C8-BTBT thickness deposited on LSMO. The O 1s and Mn $2p_{1/2}$ of (c) 80 Å and (d) 120 Å C8-BTBT thickness deposited on LSMO. Y1: 80 Å C8-BTBT before UPS test, Y1a: 80 Å C8-BTBT after UPS test; Y2: 120 Å C8-BTBT before UPS test, Y2a: 120 Å C8-BTBT after UPS test.

diffuses into the C8-BTBT film and react with C8-BTBT molecule during in the XPS test. We test the S 2p core level twice after UPS test, that is to say, the sample is constantly exposed to X-ray and the time interval between the two XPS tests is about 1 h. The S 2p core level is overlap almost completely (see supporting information Fig. S3), indicating that oxygen do not react directly with C8-BTBT molecule under the X-ray.

Jeong et al. report the chemical degradation of poly(3-hexlythiophene) (P3HT) by photo-oxidation [50] during the UPS test. One possible reaction route is the activated oxygen react with sp^2 bonds and generate sp^3 bonds with hydroxyl groups and carbonyl groups [51,52]. Another possible reaction route is the activated oxygen form ether first and detach the grafted hexyl groups [53–55]. The C8-BTBT molecule contains a BTBT core which has the same unit with P3HT, and two alkyl chain at both ends. Therefore, we cannot exclude the possibility that the oxygen diffuse from LSMO to the C8-BTBT film and react with C8-BTBT molecule under the UV light during UPS test. On the other hand, we did mention that there was a broadening in the O 1s peak in the lower binding energy side, but our resolution does not allow us to resolve a new component. Based on the peak position and composition changes and referred to the photo-oxidation in similar molecular systems [50,54], we propose a chemical reaction pathway in Scheme S1. At first, electrons transfer from O2- to Mn4+, leading to the generation of atomic oxygen. Then the O atom diffuses to C8-BTBT and reacts with C8-BTBT molecule under the UV illumination. By relaxation the electron density is likely redistributed to form a charge transfer complex (CTC) between O and C8-BTBT (CTC-C8/O). The proposed pathway is supported by the increase of Mn3+ and the formation of new components in C8-BTBT under UV illumination, but the details of the reactions may need further investigations.

4. Conclusions

In conclusion, we have investigated the evolution of the electronic structure of the 8-BTBT/LSMO interface with C8-BTBT film thickness increasing by using UPS and XPS. The results show that there is an interfacial dipole of 0.41 eV pointing from LSMO to C8-BTBT side and the near mid-gap position of the Fermi level in C8-BTBT at the interface indicates that it is difficult to inject charge from LSMO into C8-BTBT. The oxygen diffuse from LSMO to the C8-BTBT film lead to the Mn^{4+} reduction to Mn^{3+} in the C8-BTBT/LSMO interface and react with C8-BTBT molecule under ultraviolet light. The growth mode of C8-BTBT molecules is SK mode. Our results reveal the complex processes in C8-BTBT/LSMO interface and suggest a modification layer between C8-BTBT and LSMO to improve the injection efficiency.

CRediT authorship contribution statement

Haipeng Xie: Conceptualization, Methodology, Writing - original draft, Funding acquisition. **Dongmei Niu:** Writing - review & editing, Project administration, Data curation. **Yuan Zhao:** Formal analysis, Visualization. **Shitang Wang:** Formal analysis, Visualization. **Baoxing Liu:** Investigation. **Yuquan Liu:** Investigation. **Han Huang:** Writing - review & editing. **Peng Wang:** Resources. **Di Wu:** Resources, Writing - review & editing. **Yongli Gao:** Writing - review & editing, Supervision, Funding acquisition.

Declaration of Competing Interest

The authors declared that they have no conflicts of interest to this work. We declare that we do not have any commercial or associative

interest that represents a conflict of interest in connection with the work submitted.

Acknowledgements

We thank Professor Jin Liu for helpful discussions. We thank the financial support by the National Key Research and Development Program of China (Grant Nos. 2017YFA0206602), the National Natural Science Foundation of China (Grant Nos. 11334014and51802355), and National Key Laboratory Open Project Foundation (Grant No. 165000001). H.X. acknowledges the support by the Natural Science Foundation of Hunan Province (Grant No. 2018JJ3625). Y. G. acknowledges the support from National Science Foundation (DMR-1903981 and 1903962).

Appendix A. Supplementary data

Supplementary material related to this article can be found, in the online version, at doi:https://doi.org/10.1016/j.synthmet.2019.116261.

References

[1] H. Klauk, U. Zschieschang, J. Pflaum, M. Halik, Ultralow-power organic complementary circuits, Nature 445 (2007) 745–748, https://doi.org/10.1038/nature05533.
[2] C.W. Tang, Two-layer organic photovoltaic cell, Appl. Phys. Lett. 48 (1986) 183, https://doi.org/10.1063/1.96937.
[3] C.W. Tang, S.A. VanSlyke, Organic electroluminescent diodes, Appl. Phys. Lett. 51 (1987) 913, https://doi.org/10.1063/1.98799.
[4] T.D. Nguyen, G. Hukic-Markosian, F.J. Wang, L. Wojcik, X.G. Li, E. Ehrenfreund, Z.V. Vardeny, The hyperfine interaction role in the spin response of π-Conjugated polymer films and spin valve devices, Synthetic Met. 161 (2011) 598, https://doi.org/10.1016/j.synthmet.2010.12.013.
[5] N.A. Morley, A. Rao, D. Dhandapani, M.R.J. Gibbs, M. Grell, T. Richardson, Room temperature organic spintronics, J. Appl. Phys. 103 (2008) 07F306, , https://doi.org/10.1063/1.2829245.
[6] A.J. Drew, J. Hoppler, L. Schulz, F.L. Pratt, P. Desai, P. Shakya, T. Kreouzis, W.P. Gillin, A. Suter, N.A. Morley, V.K. Malik, A. Dubroka, K.W. Kim, H. Bouyanfif, F. Bourqui, C. Bernhard, R. Scheuermann, G.J. Nieuwenhuys, T. Prokscha, E. Morenzoni, Direct measurement of the electronic spin diffusion length in a fully functional organic spin valve by low-energy muon spin rotation, Nat. Mater. 8 (2009) 109, https://doi.org/10.1038/nmat2333.
[7] M. Cinchetti, K. Heimer, J.-P. Wüstenberg, O. Andreyev, M. Bauer, S. Lach, C. Ziegler, Y. Gao, M. Aeschlimann, Determination of spin injection and transport in a ferromagnet/organic semiconductor heterojunction by two-photon photoemission, Nat. Mater. 8 (2009) 115, https://doi.org/10.1038/nmat2334.
[8] H. Ding, Y. Gao, M. Cinchetti, J.-P. Wustenberg, M. Sanchez-Albaneda, O. Andreyev, M. Bauer, M. Aeschlimann, Spin injection and spin dynamics at the CuPc/GaAs interface, Phys. Rev. B 78 (2008) 075311, , https://doi.org/10.1103/PhysRevB.78.075311.
[9] Z. Valy Vardeny, Spintronics: organics strike back, Nat. Mater. 8 (2009) 91, https://doi.org/10.1038/nmat2366.
[10] I. Zutic, J. Fabian, S.D. Sarma, Spintronics: fundamentals and applications, Rev. Mod. Phys. 76 (2004) 323, https://doi.org/10.1103/RevModPhys.76.323.
[11] W.J.M. Naber, S. Faez, W.G. van der Wiel, Organic spintronics, J. Phys. D 40 (2007) R205, https://doi.org/10.1088/0022-3727/40/12/R01.
[12] S. Sanvito, Molecular spintronics, Chem. Soc. Rev. 40 (2011) 3336–3355, https://doi.org/10.1039/C1CS15047B.
[13] A.J. Drew, G. Szulczewski, L. Nuccio, W.P. Gillin, The role of interfaces in organic spin valves revealed through spectroscopic and transport measurements, Phys. Status Solidi B 249 (2012) 9–17, https://doi.org/10.1002/pssb.201147157.
[14] A. Riminucci, M. Prezioso, C. Pernechele, P. Graziosi, I. Bergenti, R. Cecchini, M. Calbucci, M. Solzi, V.A. Dediu, Hanle effect missing in a prototypical organic spintronic device, Appl. Phys. Lett. 102 (2013) 092407, , https://doi.org/10.1063/1.4794408.
[15] M. Grunewald, R. Gockeritz, N. Homonnay, F. Wurthner, L.W. Molenkamp, G. Schmidt, Vertical organic spin valves in perpendicular magnetic fields, Phys. Rev. B 88 (2013) 085319, , https://doi.org/10.1103/PhysRevB.88.085319.
[16] Y.B. Yuan, G. Giri, A.L. Ayzner, A.P. Zoombelt, S.C.B. Mannsfeld, J.H. Chen, D. Nordlund, M.F. Toney, J.S. Huang, Z.N. Bao, Ultra-high mobility transparent organic thin film transistors grown by an off-centre spin-coating method, Nat. Commun. 5 (2014) 3005, https://doi.org/10.1038/ncomms4005.
[17] R. Janneck, N. Pilet, S.P. Bommanaboyena, B. Watts, P. Heremans, J. Genoe, C. Rolin, Highly crystalline C8-BTBT thin film transistors by lateral Homo Epitaxial growth on printed templates, Adv. Mater. 27 (2017) 1703864, , https://doi.org/10.1002/adma.201703864.
[18] Y.L. Huang, J. Sun, J.D. Zhang, S.T. Wang, H. Huang, J. Zhang, D.H. Yan, Y.L. Gao, J.L. Yang, Controllable thin-film morphology and structure for 2, 7-dioctyl[1] benzothieno [3, 2-b][1]benzothiophene (C8-BTBT) based organic field-effect transistors, Org. Electron. 36 (2016) 73–81, https://doi.org/10.1016/j.orgel.2016.05.019.
[19] J.M. Adhikari, K. Vakhshouri, B.D. Calitree, A. Hexemer, M. Hickner, E.D. Gomez, Controlling crystallization to improve charge mobilities in transistors based on 2,7-dioctyl[1]benzothieno[3,2-b][1]benzothiophene, J. Mater. Chem. C 3 (2015) 8799–8803, https://doi.org/10.1039/C5TC01253H.
[20] S.C. Tong, J. Sun, C.H. Wang, Y.L. Huang, C.J. Zhang, J.Q. Shen, H.P. Xie, D.M. Niu, S. Xiao, Y.B. Yuan, J. He, J.L. Yang, Y.L. Gao, High-performance broadband perovskite photodetectors based on CH3NH3PbI3/C8-BTBT heterojunction, Adv. Electron. Mater. 3 (2017) 1700058, , https://doi.org/10.1002/aelm.201700058.
[21] J.Y. Xi, M.Q. Long, L. Tang, D. Wang, Z.G. Shuai, First-principles prediction of charge mobility in carbon and organic nanomaterials, Nanoscale 4 (2012) 4348–4369, https://doi.org/10.1039/C2NR30585B.
[22] D.L. Sun, L.F. Yin, C.J. Sun, H.W. Guo, Z. Gai, X.G. Zhang, T.Z. Ward, Z.H. Cheng, J.A. Shen, Giant magnetoresistance in organic spin valves, Phys. Rev. Lett. 104 (2010) 236602, , https://doi.org/10.1103/PhysRevLett.104.236602.
[23] R.J. Soulen Jr, J.M. Byers, M.S. Osofsky, B. Nadgorny, T. Ambrose, S.F. Cheng, P.R. Broussard, C.T. Tanaka, J. Nowak, J.S. Moodera, A. Barry, J.M.D. Coey, Measuring the spin polarization of a metal with a superconducting point contact, Science 282 (1998) 85–88, https://doi.org/10.1126/science.282.5386.85.
[24] V.N. Krivoruchko, A.I. D'yachenko, V.Y. Tarenkov, Point-contact andreev-reflection spectroscopy of doped manganites charge carrier spin-polarization and proximity effects, Low Temp. Phys. 39 (2013) 211, https://doi.org/10.1063/1.4795172.
[25] S. Majumdar, H. Huhtinen, H.S. Majumdar, R. Laiho, R. Osterbacka, Effect of $La_{0.67}Sr_{0.33}MnO_3$ electrodes on organic spin valves, J. Appl. Phys. 104 (2008) 033910, , https://doi.org/10.1063/1.2963814.
[26] Z.H. Xiong, D. Wu, Z.V. Vardeny, J. Shi, Giant magnetoresistance in organic spin-valves, Nature 427 (2004) 821–824, https://doi.org/10.1038/nature02325.
[27] J.H. Park, E. Vescovo, H.J. Kim, C. Kwon, R. Ramesh, T. Venkatesan, Magnetic properties at surface boundary of a half-metallic ferromagnet $La_{0.7}Sr_{0.3}MnO_3$, Phys. Rev. Lett. 81 (1998) 1953, https://doi.org/10.1103/PhysRevLett.81.1953.
[28] M. Bowen, M. Bibes, A. Barthelemy, J.-P. Contour, A. Anane, Y. Lemaitre, A. Fert, Nearly total spin polarization in $La_{2/3}Sr_{1/3}MnO_3$ from tunneling experiments, Appl. Phys. Lett. 82 (2003) 233, https://doi.org/10.1063/1.1534619.
[29] F.J. Yue, Y.J. Shi, B.B. Chen, H.F. Ding, F.M. Zhang, D. Wu, Manipulating spin injection into organic materials through interface engineering, Appl. Phys. Lett. 101 (2012) 022416, , https://doi.org/10.1063/1.4737008.
[30] H.P. Xie, D.M. Niu, L. Lyu, H. Zhang, Y.H. Zhang, P. Liu, P. Wang, D. Wu, Y.L. Gao, Evolution of the electronic structure of $C_{60}/La_{0.67}Sr_{0.33}MnO_3$ interface, Appl. Phys. Lett. 108 (2016) 011603, , https://doi.org/10.1063/1.4939457.
[31] K. Horiba, A. Chikamatsu, H. Kumigashira, M. Oshima, N. Nakagawa, M. Lippmaa, K. Ono, M. Kawasaki, H. Koinuma, In vacuo photoemission study of atomically controlled $La_{1-x}Sr_xMnO_3$ thin films: composition dependence of the electronic structure, Phys. Rev. B 71 (2005) 155420, , https://doi.org/10.1103/PhysRevB.71.155420.
[32] M. Grobosch, K. Dorr, R.B. Gangineni, M. Knupfer, Energy level alignment and interactions at potential contacts for spin injection into organic semiconductors, Adv. Eng. Mater. 11 (2009) 285, https://doi.org/10.1002/adem.200800240.
[33] Y.Q. Zhan, I. Bergenti, L.E. Hueso, V. Dediu, M.P. de Jong, Z.S. Li, Alignment of energy levels at the $Alq_3/La_{0.7}Sr_{0.3}MnO_3$ interface for organic spintronic devices, Phys. Rev. B 76 (2007) 045406, , https://doi.org/10.1103/PhysRevB.76.045406.
[34] L. Lyu, D.M. Niu, H.P. Xie, Y. Zhao, N.T. Cao, H. Zhang, Y.H. Zhang, P. Liu, Y.L. Gao, The correlations of the electronic structure and film growth of 2,7-diocty [1]benzothieno[3,2-b]benzothiophene (C8-BTBT) on SiO_2, Phys. Chem. Chem. Phys. 19 (2017) 1669–1676, https://doi.org/10.1039/C6CP06919C.
[35] L. Lyu, D.M. Niu, H.P. Xie, N.T. Cao, H. Zhang, Y.H. Zhang, P. Liu, Y.L. Gao, Orientation-dependent energy level alignment and film growth of 2,7-diocty[1] benzothieno[3,2-b]benzothiophene (C8-BTBT) on HOPG, J. Chem. Phys. 144 (2016) 034701, , https://doi.org/10.1063/1.4939839.
[36] S. Duhm, H. Glowatzki, J.P. Rabe, N. Koch, R.L. Johnson, Influence of alkyl chain substitution on sexithienyl-metal interface morphology and energetics, Appl. Phys. Lett. 88 (2006) 203109, , https://doi.org/10.1063/1.2204834.
[37] C.E. Heiner, J. Dreyer, I.V. Hertel, N. Koch, H.-H. Ritze, W. Widdra, B. Winter, Anisotropy in ordered sexithiophene thin films studied by angle-resolved photoemission using combined laser and synchrotron radiation, Appl. Phys. Lett. 87 (2005) 093501, , https://doi.org/10.1063/1.2034105.
[38] H. Kobayashi, N. Kobayashi, S. Hosoi, N. Koshitani, D. Murakami, R. Shirasawa, Y. Kudo, D. Hobara, Y. Tokita, M. Itabashi, Hopping and band mobilities ofPentacene, Rubrene, and 2,7-dioctyl[1]benzothieno[3,2-b][1]benzothiophene (C8-BTBT) from first principle calculations, J. Chem. Phys. 139 (2013) 014707, , https://doi.org/10.1063/1.4812389.
[39] Y. Gao, Surface analytical studies of interfaces in organic semiconductor devices, Mater. Sci. Eng., R 68 (2010) 39–87, https://doi.org/10.1016/j.mser.2010.01.001.
[40] H. Zhang, D.M. Niu, L. Lyu, H.P. Xie, Y.H. Zhang, P. Liu, H. Huang, Y.L. Gao, Thickness dependence of interface electronic structure in C8-BTBT/Ni(100), Acta Phys. Sin. 65 (2016) 047902http://wulixb.iphy.ac.cn/EN/10.7498/aps.65.047902.
[41] Y.H. Zhang, D.M. Niu, L. Lü, H.P. Xie, M.L. Zhu, H. Zhang, P. Liu, N.T. Cao, Y.L. Gao, Adsorption, film growth, and electronic structures of 2,7-dioctyl[1]benzothieno-[3,2-b][1]benzothiophene (C8-BTBT) on Cu(100), Acta Phys. Sin. 65 (2016) 157901 http://wulixb.iphy.ac.cn/EN/10.7498/aps.65.157901.
[42] S. Ponce, M.A. Pena, J.L.G. Fierro, Surface properties and catalytic performance in methane combustion of Sr-Substituted lanthanum manganites, Appl. Catal. B 24 (2000) 193, https://doi.org/10.1016/S0926-3373(99)00111-3.
[43] Y.C. Liang, H. Zhong, Materials synthesis and annealing-induced changes of microstructure, Appl. Surf. Sci. 283 (2013) 490, https://doi.org/10.1016/j.apsusc.

2013.06.134.
[44] H.P. Xie, H. Huang, T.N. Cao, C.H. Zhou, D.M. Niu, Y.L. Gao, Effects of annealing on structure and composition of LSMO thin films, Physica B 477 (2015) 14, https://doi.org/10.1016/j.physb.2015.07.032.
[45] E. Beyreuther, S. Grafstrom, L.M. Eng, C. Thiele, K. Dorr, XPS investigation of Mn Valence in lanthanum manganite thin films under variation of oxygen content, Phys. Rev. B 73 (2006) 155425, , https://doi.org/10.1103/PhysRevB.73.155425.
[46] E.J. Crumlin, E. Mutoro, Z. Liu, M.E. Grass, M.D. Biegalski, Y.L. Lee, D. Morgan, H.M. Christen, H. Bluhm, Y. Shao-Horn, Surface strontium enrichment on highly active perovskites for oxygen electrocatalysis in solid oxide fuel cells, Energy Environ. Sci. 5 (2012) 6081–6088, https://doi.org/10.1039/C2EE03397F.
[47] M.L. Zhu, L. Lyu, D.M. Niu, H. Zhang, S.T. Wang, Y.L. Gao, Effect of a MoO_3 buffer layer between C8-BTBT and Co(100) single-crystal film, RSC Adv. 6 (2016) 112403, , https://doi.org/10.1039/C6RA23981A.
[48] G. Greczynski, T. Kugler, M. Keil, W. Osikowicz, M. Fahlman, W.R. Salaneck, Photoelectron spectroscopy of thin films of PEDOT-PSS conjugated polymer blend: a mini-review and some new results, J. Electron. Spectrosc. Relat. Phenom. 121 (2001) 1–17, https://doi.org/10.1016/S0368-2048(01)00323-1.
[49] A. Dettlaff, M. Wilamowska, Electrochemical synthesis and characterization of nanocomposites based on poly(3,4-ethylenedioxythiophene) and functionalized carbon nanotubes, Synthetic Met. 212 (2016) 31–43, https://doi.org/10.1016/j.synthmet.2015.11.030.
[50] J.Y. Oh, M. Shin, H.W. Lee, Y.J. Lee, H.K. Baik, U. Jeong, Enhanced air stability of polymer solar cells with a nanofibril-based photoactive layer, ACS Appl. Mater. Interfaces 6 (2014) 7759–7765, https://doi.org/10.1021/am501034g.
[51] M. Jørgense, K. Norrman, F.C. Kebs, Stability/Degradation of polymer solar cells, Sol. Energy Mater. Sol. Cells 92 (2008) 686–714, https://doi.org/10.1016/j.solmat.2008.01.005.
[52] M.G. Matturro, R.P. Reynolds, R.V. Kastrup, C.F. Pictroski, Thioozonide decomposition: sulfur and oxygen atom transfer. Evidence for the formation of a carbonyl O-Sulfide intermediate, J. Am. Chem. Soc. 108 (1986) 2775–2776, https://doi.org/10.1021/ja00270a058.
[53] H. Hintz, H.-J. Egelhaaf, L. Lüer, H. Hauch, H. Peisert, T. Chasse, Photodegradation of P3HT-A systematic study of environmental factors, Chem. Mater. 23 (2011) 145, https://doi.org/10.1021/cm102373k.
[54] A. Aguirre, S.C.J. Meskers, R.A.J. Janssen, H.-J. Egelhaaf, Formation of metastable charges as a first step in photoinduced degradation in π-conjugated polymer: fullerene blends for photovoltaic applications, Org. Electron. 12 (2011) 1657, https://doi.org/10.1016/j.orgel.2011.06.020.
[55] H. Hintz, H.-J. Egelhaaf, H. Peisert, T. Chasse, Photo-oxidation and ozonization of poly(3-hexylthiophene) thin films as studied by UV/VIS and photoelectron spectroscopy, Polym. Degrad. Stab. 95 (2010) 818, https://doi.org/10.1016/j.polymdegradstab.2010.02.004.